

## Emission of O I(630 nm) in proton aurora

D. Lummerzheim<sup>1</sup>, M. Galand,<sup>2,3</sup> J. Semeter,<sup>4</sup> M. J. Mendillo,<sup>3</sup> M. H. Rees,<sup>5</sup> and F. J. Rich<sup>6</sup>

**Abstract.** A red aurora occurred over southern Canada and central Maine on April 11, 1997, producing a brightness of O I(630 nm) of several Kilorayleighs, which lasted for several hours. Two passes of the Defense Meteorological Satellite Program (DMSP) F12 satellite occurred during this time, and optical data were obtained from four CEDAR Optical Tomographic Imaging Facility (COTIF) sites. The DMSP F12 particle spectrometers observed proton precipitation south of the electron aurora with energy fluxes of several  $\text{mW m}^{-2}$ . Tomographic inversion of the COTIF optical observations gives the altitude profile of emissions along a magnetic meridian. We combine all available data using an ionospheric auroral model. Our analysis shows that the model produces the observed auroral brightness from the proton precipitation alone.

### 1. Introduction

The appearance of proton aurora from the ground is typically that of a dim and diffuse glow. Unlike electron aurora, which occurs as bright and well-defined curtains, proton aurora tends to have very little structure in the observed brightness. This is because of the horizontal spreading of the precipitating energetic particles. Energetic protons, which are bound to gyrate around the geomagnetic field lines, readily undergo charge exchange in collisions with atmospheric neutrals. The resulting energetic hydrogen continues on a straight path in the direction given by the pitch angle and azimuth angle of the gyration of the proton at the moment of the collision. Subsequent stripping collisions of the energetic hydrogen with atmospheric neutrals returns an energetic proton again. This process leads to the horizontal spreading and loss of structure that the original energetic proton flux may have had.

The horizontal spreading also causes a significant de-

crease of the observable brightness of optical emissions in proton aurora compared to an electron aurora with the same total energy flux. An optical signature of proton aurora is the brightness of hydrogen emissions,  $\text{H}_\alpha$  at 656.3 nm and  $\text{H}_\beta$  at 486.1 nm in the visible wavelength range and Lyman- $\alpha$  in the extreme ultraviolet wavelength range. These hydrogen emissions do not occur in electron aurora, because of the small fraction of hydrogen in the neutral atmosphere. The energetic hydrogen that emerges from charge-exchange collisions, on the other hand, will be excited and emit Doppler-shifted radiation of hydrogen lines. The energetic hydrogen atoms and protons also cause excitation and ionization in collisions with the neutral constituents in the atmosphere. The secondary electrons (by this we mean the ejected electrons in ionization collisions) also have sufficient energy for further excitation and ionization. They are an additional source for the excitation of  $\text{N}_2$ ,  $\text{O}_2$ , and O that leads to the full spectrum of auroral emissions in proton aurora.

Optical emissions in the UV and EUV spectral range in proton aurora have been studied systematically by *Strickland et al.* [1993]. *Rees* [1982] has calculated the  $\text{H}_\alpha$  and  $\text{H}_\beta$  brightness in relation to the  $\text{N}_2^+$  first negative (1 N) brightness to compare theoretical predictions of brightness ratios to observed values. *Edgar et al.* [1975] studied red line emissions in the polar cap that result from high energy (MeV) proton precipitation. *Sri-*

---

<sup>1</sup>Geophysical Institute, University of Alaska, Fairbanks.

<sup>2</sup>Space Environment Center, NOAA, Boulder, Colorado.

<sup>3</sup>Center for Space Physics, Boston University, Boston, Massachusetts.

<sup>4</sup>SRI International, Menlo Park, California.

<sup>5</sup>Physics Department, Southampton University, Southampton, England, United Kingdom.

<sup>6</sup>U.S. Air Force Research Laboratory, Space Vehicle Directorate, Hanscom Air Force Base, Massachusetts.

*vastava and Singh* [1988] present model calculations for the brightness of O I(630 nm) and O I(557.7 nm) for various proton precipitation spectra, including power law spectra representative for high-energy polar cap precipitation and Maxwellian spectra for proton aurora in the keV energy range. In an early paper on excitation of high-altitude red auroral arcs, *Rees* [1961] concluded that the most likely excitation source of an arc observed and measured in Alaska [*Rees and Deehr*, 1961] was a flux of several keV protons of  $\sim 10^{10} \text{ cm}^{-2} \text{ s}^{-1}$ .

In this paper we examine a specific case of proton aurora where we have good observational coverage. On April 11, 1997, a red aurora was visible north of Boston. Two Defense Meteorological Satellite Program (DMSP) F12 passes collected particle spectra during this time. The dominance of proton precipitation on the equatorward edge of the auroral oval is not uncommon and has been measured by the NOAA-TIROS satellites as well as the DMSP satellites. Ground-based observations are available from a chain of meridional imaging spectrometers and an all-sky imager. Global auroral images from Polar are available only northward of the observed aurora, because of the orbit of the satellite. Our interpretation of the data is based on model calculations using a proton-hydrogen transport code, coupled with an electron transport code and an ionospheric auroral model.

Of course, red aurora is not always caused by energetic proton precipitation. Indeed, a flux of soft electrons usually is responsible for the long-lived emission of O(<sup>1</sup>D) atoms. Since both proton and soft electron precipitation are capable of producing red aurora, the particle measurements are essential for a correct interpretation of the optical observations.

## 2. Observations

Ground-based optical observations were obtained from the CEDAR Optical Tomographic Imaging Facility (COTIF). The COTIF observing sites are located along the New England coast between Rhode Island and Maine. This places the stations at magnetic latitudes which are usually equatorward of the auroral oval. During active periods the aurora can expand far enough equatorward to be in the zenith above the COTIF chain. The alignment of the COTIF observing sites allows a two-dimensional tomographic inversion of selected emission rates. On April 11, 1997, the auroral oval expanded considerably and was well in the field of view of the COTIF imagers. *Semeter et al.* [1999] have analyzed the data for this event with their tomographic inversion technique [*Semeter and Mendillo*, 1997] and have recon-

structed the volume emission rates of the O I(630 nm) emission for the period from 0300 to 0315 UT.

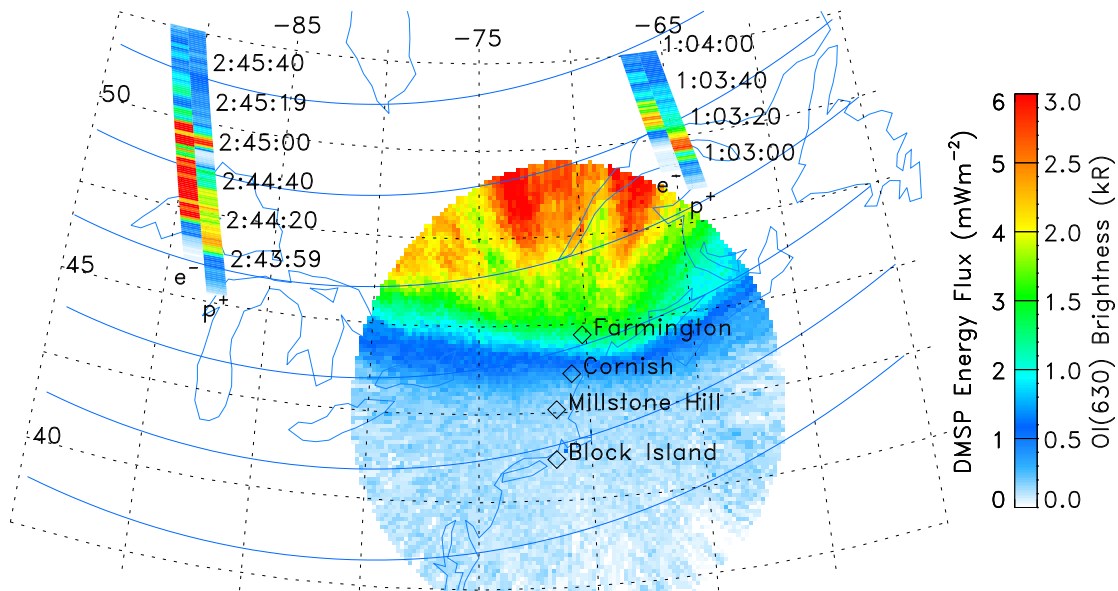
As part of COTIF, a monochromatic all-sky camera was operated at Millstone Hill to obtain two-dimensional images of the O I(630 nm) brightness. All-sky images provide a valuable spatial context for data interpretation. To relate the all-sky images to other data locations, we have mapped the images assuming a single emission altitude of 250 km. Plate 1 shows such an image recorded during the period of maximum equatorial expansion at 0307 UT.

Two DMSP F12 passes occurred in the vicinity of the COTIF observations while the auroral emissions moved south. We obtained electron and proton particle spectra from these two passes. Both passes show a significant proton energy flux equatorward of the region of electron precipitation. Colocated with the proton precipitation region is a region of very rapid westward ion flow, indicative of a Sub-Auroral Ion Drift (SAID) event.

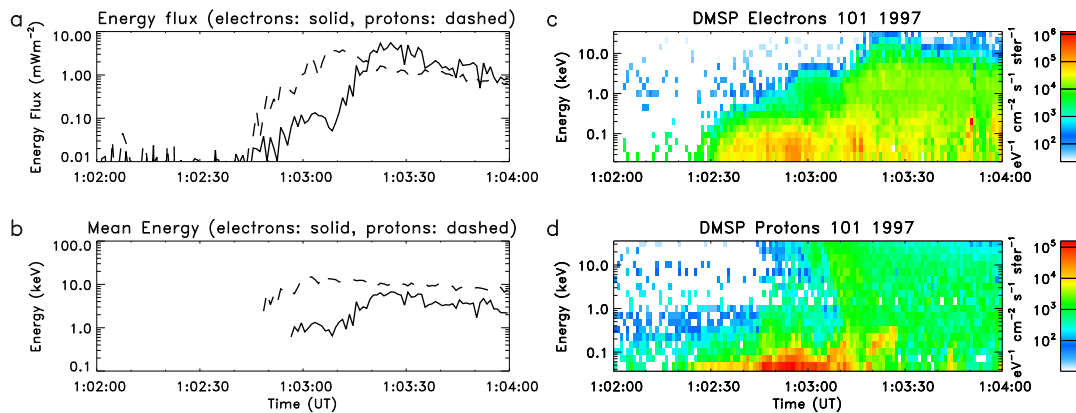
Our analysis focuses on the time period when the COTIF reconstructed volume emission rate can best be done, namely, when the auroral emissions are present between stations. The two DMSP F12 passes occurred at 0103 UT and 0244 UT, 2 hours and 20 min before this time, respectively. Plate 1 shows the electron and proton energy fluxes as color-coded strips, mapped along the magnetic field to an altitude of 250 km. The color scale is given in Plate 1. The proton energy flux is plotted to the right side of the flight path; the electron energy flux is plotted to the left side. For both passes one can clearly see the proton flux at the southern edge of the electron aurora.

Plate 2 shows an energy spectrogram and integrated number and energy fluxes for protons and electrons for the first pass at 0103 UT. The energy flux and mean energy of the protons at the southern edge of the aurora during the second pass at 0244 UT are very similar. Since similar proton precipitation appears in both passes, separated by 90 min, we assume that the proton flux 20 min after the second pass can be represented by the same particle spectra as observed on these two passes.

The blue lines on the map in Plate 1 show lines of constant magnetic latitude. The area of proton precipitation is farther north (in both magnetic and geographic latitudes) in the first pass compared to the 0244 UT pass. The COTIF tomographic reconstruction is done for a time 20 min after the second DMSP F12 pass. The all-sky image shows the location of the aurora at that time (0307 UT). It is reasonable to assume that the aurora kept moving south, such that the area of proton



**Plate 1.** Map showing the relative location of the satellite and ground-based observations. The proton and electron energy fluxes along the DMSP F12 passes are shown as a color-coded strip (protons to the right, electrons to the left side of each pass). The color bar applies to both protons and electrons. The CEDAR Optical Tomographic Imaging Facility (COTIF) locations are indicated, and the OI(630 nm) Millstone Hill all-sky image from 0307 UT is shown mapped to 250-km altitude. Lines of constant magnetic latitude with  $2.5^\circ$  spacing from  $50^\circ$  to  $62.5^\circ$  are shown in blue. The DMSP passes were 2 hours and 20 min, respectively, before the aurora reached the COTIF sites.



**Plate 2.** DMSP F12 electron and proton spectrograms. (a) The integrated energy flux (solid line for electrons, dashed line for protons). (b) The mean energy of electrons and protons. We only calculate the mean energy where the energy flux is above  $0.05 \text{ mW m}^{-2}$ . (c) The electron spectrograms. (d) The proton spectrograms.

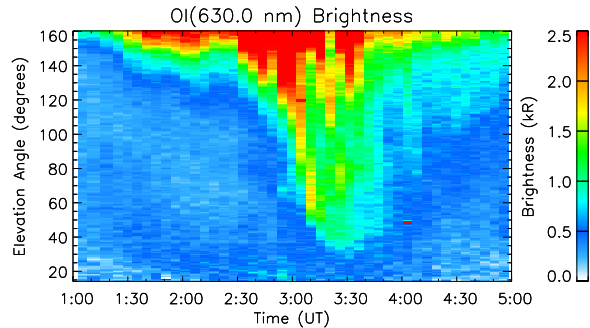


**Plate 3.** Meridional brightness versus time of the OI(630 nm) red line brightness from Farmington. Shown is the line of sight brightness as a function of elevation angle (bottom is south, top is north) and time. Note that the color scale is set to terminate at 2.5 kR, while the actual brightness in the north reached 5.5 kR.

precipitation did get into the zenith of Farmington. The COTIF spectroscopic observations of the OI(630 nm) brightness from the Farmington imaging spectrometer, shown in Plate 3, also show the southward motion of the southern edge of the auroral brightness.

We thus assume that the proton particle spectrum measured by the DMSP F12 satellite near 0244 UT and near 0103 UT is representative for the precipitation in the zenith of Farmington between 0300 and 0315 UT. We use these representative spectra as input to our auroral model.

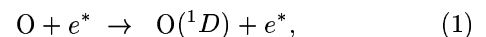
### 3. Auroral Model

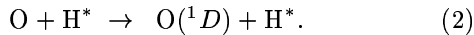
Modeling of proton aurora requires a transport model that solves the transport and energy degradation of the coupled proton and hydrogen fluxes. There are several approaches that have been used for this problem. Monte Carlo simulations are best suited to include the horizontal spreading as the numerical effort for a two- or three-dimensional code is not much greater than that for one dimensional codes. *Davidson* [1965] showed that the proton aurora from a single source spreads over several hundred kilometers. New cross-section measurements are included in more recent models [*Kozelov and Ivanov*, 1992; *Kozelov*, 1993; *Decker et al.*, 1996; *Sigernes*, 1996; *Sigernes et al.*, 1996; *Lorentzen et al.*, 1998; *Synnes et al.*, 1998] which predict similar spreading. One-dimensional models include an assumed correction factor [*Jasperse and Basu*, 1982] to account for the spreading. Several other methods are used to solve the one-dimensional transport equation. *Jasperse and*

*Basu* [1982] use a theoretical approach while others have presented numerical methods [*Basu et al.*, 1987, 1993; *Strickland et al.*, 1993; *Galand et al.*, 1997, 1998].

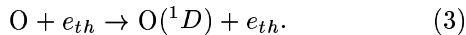
The optical emissions, other than the hydrogen emissions themselves, have significant contributions from excitation by the secondary electrons that are generated in ionization collisions. In particular, the emissions originating from excited states with a low excitation energy threshold are dominated by the secondary electrons. *Strickland et al.* [1993] have coupled the proton-hydrogen transport with electron transport to properly account for the secondary electrons. The energy spectrum of the secondary electrons is different from those of secondary electrons in electron aurora [*Rudd*, 1979; *Basu et al.*, 1993] and thus may lead to different brightness ratios of auroral emissions [*Srivastava and Singh*, 1988]. The secondary electrons in proton aurora have a lower mean energy than those in electron aurora, which should lead to relatively brighter red line emissions. In this study we have combined the proton-hydrogen transport model from *Galand et al.* [1997] with the electron transport model by *Lummerzheim and Lilensten* [1994]. This combined transport calculation is embedded in an ionospheric model which solves the ion continuity equations to obtain the ionospheric plasma density and which solves the electron energy equation to obtain the electron temperature. The neutral density and temperature are not affected by the precipitation and are prescribed by the Mass Spectrometer and Incoherent Scatter (MSIS) [*Hedin*, 1991] density and temperature profiles. For our case study we generated an MSIS atmosphere for the location of Farmington with a magnetic activity index  $ap = 37$  and solar flux  $F_{10.7} = 77.4$  (90 days average of 73) to represent the actual conditions. The transport calculation and auroral model are one-dimensional along the direction of the magnetic field (dip angle is  $70^\circ$  at Farmington), but we present our results as a function of altitude.

Both proton-hydrogen impact and electron impact on neutral atmospheric constituents provide sources for excited states. The brightness of spontaneous emissions, like the  $N_2^+(1N)$ , can be determined directly from the excitation rate. To obtain the brightness of the oxygen red line OI(630 nm) we include several competing excitation and de-excitation mechanisms in our auroral model. We have direct excitation by electron and hydrogen atom impact using cross sections as discussed by *Lummerzheim and Lilensten* [1994] for electron impact and *Edgar et al.* [1975] for hydrogen impact:

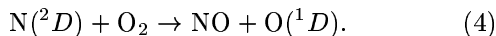




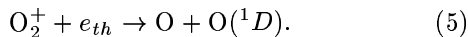
The excitation of  $\text{O}({}^1D)$  by proton impact on  $\text{O}$  requires spin exchange and is therefore highly unlikely. Heating of the ionospheric plasma in aurora can also contribute to the excitation of the  $\text{O}({}^1D)$  state, which has a threshold energy of 1.92 eV. The high-energy tail of the thermal electron gas can extend above this energy and contribute to excitation. For our model we have adopted the same parameterization of the thermal excitation as is used in the Thermosphere-Ionosphere-Mesosphere-Electrodynamics General Circulation Model (TIME-GCM) [Roble, 1996]:



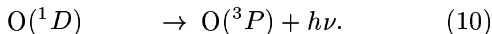
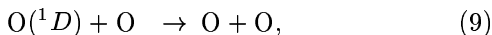
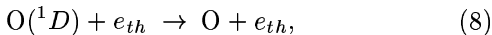
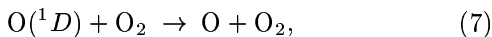
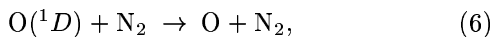
Following Rees and Roble [1986], we include the reaction of  $\text{N}({}^2D)$  with  $\text{O}_2$  which yields  $\text{O}({}^1D)$ , using a reaction rate coefficient of  $5.3 \times 10^{-12} \text{ cm}^3 \text{ s}^{-1}$ . The  $\text{N}({}^2D)$  results from dissociation and recombination of  $\text{N}_2^+$  and  $\text{NO}^+$ , which in turn are excited by particle impact and subsequent ion-chemical reactions in aurora [Rees, 1989]:



Finally, we include dissociative recombination.  $\text{O}_2^+$  results from ionization by particle impact and leads to  $\text{O}({}^1D)$  by recombination:



The radiative lifetime of the excited  $\text{O}({}^1D)$  state is 107 s. De-excitation is thus not only by radiation but by various collisional processes:



The relative importance of these excitation and de-excitation processes is shown in Figure 1. Figure 1 was produced using the observed DMSP proton precipitation as input to the model. Since the lifetime of the  $\text{O}({}^1D)$  state is  $\sim 100$  s, we kept the proton aurora constant for 10 min to produce a steady state condition. The direct excitation (labeled “particle impact”)

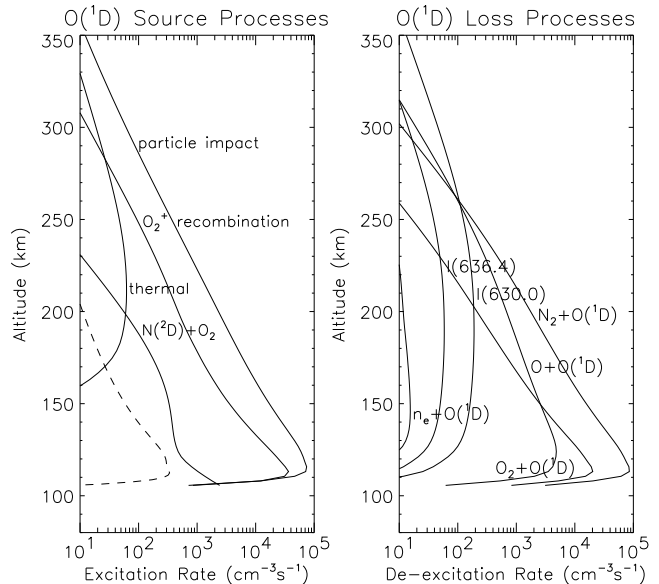


**Figure 1.** Processes that are considered in the OI(630 nm) emission calculation: (left) excitation and (right) de-excitation processes. The line labeled “particle impact” includes the sum of hydrogen and secondary electron impact on atomic oxygen; the dashed line (left panel) shows the hydrogen contribution to this total. The lines labeled “I(630.0)” and “I(636.4)” show the emission rates of the red line.

includes electron and neutral hydrogen impact on ambient atomic oxygen. The excitation from hydrogen impact produces less than 1% of the total and is shown separately as a dashed line. The dominant excitation source is impact by the secondary electrons.

#### 4. Data Analysis and Model Results

The ground-based optical data from the COTIF spectrometers were analyzed by a tomographic inversion as described by Semeter *et al.* [1999]. This allowed us to obtain altitude profiles of the emission rate of the OI(630 nm) emission. Figure 2 shows the volume emission rate as a function of latitude along the COTIF meridian and altitude at three times. Note that Plate 1 gives the impression that most of the precipitation was north of  $45^\circ$  geographic latitude. This is an artifact of the assumptions intrinsic to the transformation from elevation angle to geographic latitude of all-sky images, i.e., that the emission occurred in a thin layer and at a constant altitude (in this case, 250 km). These assumptions are particularly poor for

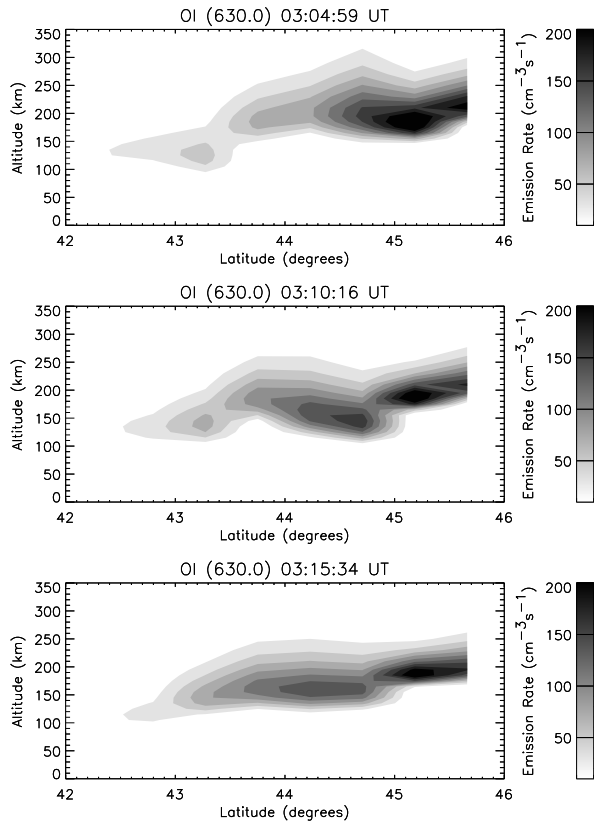


**Figure 2.** Volume emission rate of OI(630 nm) as a function of latitude and altitude reconstructed from the COTIF imaging spectrometer data. The location of Farmington is at  $44.7^\circ$  latitude.

red line emissions. The tomographic analysis summarized in Figure 2 shows that the aurora, in fact, moved into the zenith of Farmington ( $44.68^\circ$ ), where the height-integrated volume emission rate reached  $1.5 \text{ kR}$  at 0310 UT.

The particle spectra measured by the DMSP F12 satellite (Plate 2) show that the protons dominate the equatorward edge of the precipitation with energy fluxes of several  $\text{mW m}^{-2}$ . There is a substantial low-energy proton population below 100 eV, but the peak energy of the proton spectra is at or near the upper energy limit (32 keV) of the DMSP detectors (Plate 2-d at  $\sim 0103 \text{ UT}$ ). The next DMSP F12 pass shows proton precipitation with the same general characteristics. In order to construct a representative proton spectrum, we thus extrapolated the DMSP spectra by adding three artificial data points at 45, 60, and 150 keV with values of 0.7, 0.2, and 0.0001 of the peak measured proton flux. This extrapolation provides a much steeper de-

crease than Maxwellian or Kappa distribution fits to the data and ensures that the energy flux of the precipitation is dominated by the measured part of the spectrum. Figure 3 (top) shows 10 individual measured proton spectra from 0103:00 to 0103:09 UT and the averaged and extrapolated spectrum derived from them. Figure 3 (bottom) shows a similar display for the next DMSP pass from 0244:00 to 0244:09 UT. The spectrum of the precipitating protons is similar. The averaged and extrapolated spectrum was assumed to be representative of the proton precipitation and was used as input to the auroral model. The energy flux and mean energy of the protons are  $7 \text{ mW m}^{-2}$  and 28 keV, respectively.

The model produces the temporal evolution of plasma density, composition, and temperature, and various auroral emissions. We initialize the model without auroral precipitation at local noon and let it evolve in time to develop realistic ionospheric conditions before turning on the aurora. The aurora occurred over Farmington in the evening; 0300 UT corresponds to 2200 LT. The aurora in this case was moving slowly southward, and we simulate this in our one-dimensional model by turning on the precipitation at 2200 LT and extracting the emission rates after 10 min of constant proton precipitation at 2210 LT. Figure 4 shows the modeled OI(630 nm) volume emission rate as a solid line and the observed volume emission rate over Farmington as symbols. Since the measurement of precipitating particles and the measurement of the optical emissions were neither conjugate nor simultaneous, the comparison of the modeled and observed emission rate profiles should only be made in general terms. We selected the location of Farmington because these emissions originate in the equatorward edge of the observed aurora, in accordance with the relative location of the particle observations. The symbols show profiles from the three time periods of the reconstructed volume emission rate in Figure 2. The red line emission in aurora originates typically from altitudes around 250 km. Below this altitude the  $\text{O}(^1D)$  state is significantly quenched, so that large excitation rates are needed to produce red line emission. Both the model and the tomographic reconstruction show the maximum of the red line emission below 200 km with emissions extending to much lower altitudes. Comparing the emission rate to the excitation rate (Figure 1) shows that at 150-km altitude only  $\sim 1\%$  of the excitation leads to emission. The significant quenching causes the blunt profile in the model.

The modeled red line emission agrees reasonably well with the observed reconstructed profiles, even though

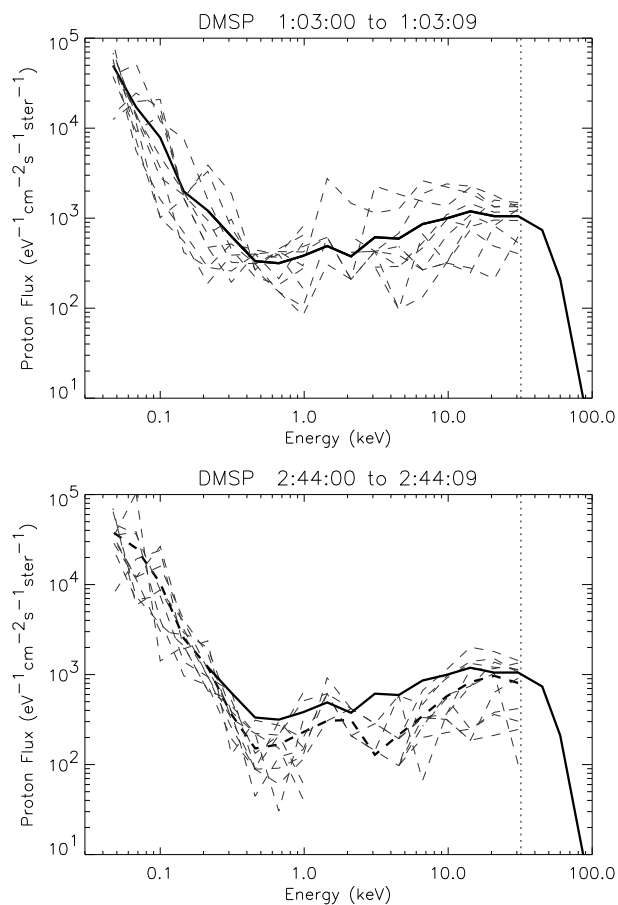


**Figure 3.** Observed proton flux while the DMSP F12 satellite was over the equatorward edge of the auroral precipitation region. (top) Display showing DMSP pass from 0103:00 to 0103:09 UT. The dashed lines show 10 individual particle spectra at 1-s intervals from 0103:00 to 0103:09 UT; the solid line is the average of these spectra. The vertical line indicates the upper energy limit of the DMSP detector. Above this energy the solid line shows our assumed extrapolation of the proton spectrum. (bottom) Similar display for the next DMSP pass at 0244:00 to 0244:09 UT. The average of the 10 individual spectra is shown by the thick dashed line; the solid line is the average from the top panel, shown for comparison.

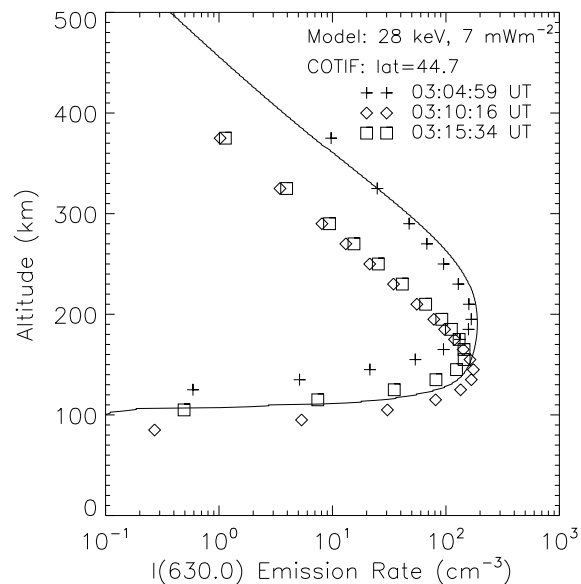


**Figure 4.** Modeled (solid line) and observed (crosses) OI(630 nm) volume emission rate over Farmington. The input to the model calculations was obtained from proton particle spectra measured at 0103 UT.

the incident proton flux is extrapolated from DMSP measurements that took place more than 20 and 120 min before the optical observation. This gives us confidence that the assumptions that went into the construction of the incident particle spectrum and the modeling are justified. The peaks of the emission of the modeled and reconstructed profiles are in the same altitude range, even though the reconstruction did not include any a priori information about the quenching of the  $O(^1D)$  state. The bottom part of the modeled and reconstructed profiles have the largest uncertainty. This is because of the assumed high-energy part of the precipitating protons and the assumptions that went into the reconstruction [Semeter *et al.*, 1999].

## 5. Summary and Conclusion

DMSP F12 particle observations of two successive passes show that the equatorward edge of the auroral precipitation region on April 11, 1997, is dominated by energetic protons. Ground-based optical observations 20 min after the second DMSP F12 pass and  $2.5^\circ$  of magnetic latitude south of the particle observations showed significant red aurora. Both DMSP particle observations and ground-based optical observations indi-

cate that the region of precipitation was moving to lower latitudes. In order to construct a particle spectrum of the precipitation, we assumed that the DMSP proton spectra would be persistent and continue to dominate the equatorward edge of the aurora. Using the DMSP proton spectra without any precipitating electrons, our auroral model reproduced the observed altitude profile of the OI(630 nm) volume emission rate over Farmington. We thus postulate that this red aurora that was visible from Boston was entirely due to proton precipitation and the secondary electrons they produce.

The extreme energy flux associated with proton precipitation in this event produced significant red line emission below 200 km. It is generally accepted that quenching efficiently reduces red line emission in this regime. The secondary electrons from ionization processes in proton aurora have lower mean energy than secondary electrons in electron aurora. Proton precipitation is thus very efficient in the indirect excitation of  $O(^1D)$ . Together with the large incident energy flux in this proton aurora, the excitation of  $O(^1D)$  at low altitudes was large enough that significant emission of the auroral red line came from altitudes as low as 150 km. This is supported by both the modeling and the tomographic reconstruction.

The auroral model also calculates other auroral emissions. We can separate the contribution to each emission from direct proton-hydrogen impact and from secondary electron impact. The necessary excitation cross sections for proton and hydrogen impact on the neutral constituents of the atmosphere are often poorly known. The presented emission rates should thus be considered as estimates. We used the cross sections that were presented by *Strickland et al.* [1993]. These cross sections are mostly based on measurements and theoretical calculations by *Van Zyl et al.* [1983] and private communications by Van Zyl as presented by *Strickland et al.* [1993]. The  $N_2^+(1N)$  emissions result mostly from direct proton-hydrogen impact ionization. The secondary electrons contribute a minor portion to the ionization, owing to their low energy. We get a  $N_2^+$  (391.4 nm) total column integrated emission rate of 9 kR, with 2 kR from the secondary electrons. The  $N_2(2PG)$  and  $N_2(LBH)$  emissions have excitation cross sections at lower energies and are dominated by the excitation from secondary electrons: total band emission of LBH is 25.4 kR, of which 20% comes from direct proton-hydrogen excitation, and emission of the (0-0) band of  $N_2(2PG)$  at 337.1 nm is 7.4 kR, with 15% from direct proton-hydrogen excitation. This compares to almost no direct contribution (1%) to the auroral red line

OI(630 nm). The relative contributions that are quoted here are from the particular case of the April 11, 1997, aurora over Maine. We have not conducted a systematic study of auroral emissions in proton aurora, and we cannot generalize conclusions from this case study. The COTIF spectroscopic imagers cover a wavelength range of 200 nm, which does not include these UV emissions. We have observations of the brightness of the auroral green line OI(557.7 nm) and of the NI(520 nm) from the forbidden  $N(^2D - ^4S)$  transition. The interpretation of these observations will be the subject of a future paper.

**Acknowledgments.** This research was supported at the University of Alaska by internal funds from the Geophysical Institute and by NOAA through the National Research Council and the Space Environment Center. Support of DMSP data analysis is provided by the Air Force Office of Scientific Research. The COTIF program at Boston University is supported by a grant from the NSF Aeronomy Program.

Janet G. Luhmann thanks Stanley C. Solomon and another referee for their assistance in evaluating this paper.

## References

- Basu, B., J. R. Jasperse, R. M. Robinson, R. R. Vondrak, and D. S. Evans, Linear transport theory of auroral proton precipitation: A comparison with observations, *J. Geophys. Res.*, *92*, 5920, 1987.
- Basu, B., J. R. Jasperse, D. J. Strickland, and R. E. Daniell Jr., Transport-theoretic model for the electron-proton-hydrogen atom aurora, 1, Theory, *J. Geophys. Res.*, *98*, 21,517, 1993.
- Davidson, T. D., Expected spatial distribution of low-energy protons precipitated in the auroral zone, *J. Geophys. Res.*, *70*, 1290, 1965.
- Decker, D. T., B. V. Kozelov, B. Basu, J. R. Jasperse, and V. E. Ivanov, Collisional degradation of the proton-H atom fluxes in the atmosphere: A comparison of theoretical techniques, *J. Geophys. Res.*, *101*, 26,947, 1996.
- Edgar, B. C., H. S. Porter, and A. E. S. Green, Proton energy deposition in molecular and atomic oxygen and application to polar cap, *Planet. Space Sci.*, *23*, 787, 1975.
- Galand, M., J. Lilensten, W. Kofman, and R.B. Sidje, Proton transport model in the ionosphere, 1, Multistream approach of the transport equations, *J. Geophys. Res.*, *102*, 22,261, 1997.
- Galand, M., J. Lilensten, W. Kofman, and D. Lummerzheim, Proton transport model in the ionosphere, 2, Influence of magnetic mirroring and collisions on the angular redistribution in a proton beam, *Ann. Geophys.*, *16*, 1308, 1998.
- Hedin, A. E., Extension of the MSIS thermosphere model into the middle and lower atmosphere, *J. Geophys. Res.*, *96*, 1159, 1991.

- Jasperse, J. R., and B. Basu, Transport theoretic solutions for aurora proton and H atom fluxes and related quantities, *J. Geophys. Res.*, *87*, 811, 1982.
- Kozelov, B. V., Influence of the dipolar magnetic field on transport of proton-H atom fluxes in the atmosphere, *Ann. Geophys.*, *11*, 697, 1993.
- Kozelov, B. V., and V. E. Ivanov, Monte-Carlo calculation of proton-hydrogen atom transport in N<sub>2</sub>, *Planet. Space Sci.*, *40*, 1503, 1992.
- Lorentzen, D. A., F. Sigernes, and C. S. Deehr, Modeling and observations of dayside auroral hydrogen emission Doppler profiles, *J. Geophys. Res.*, *103*, 17,479, 1998.
- Lummerzheim, D. and J. Liliensten, Electron transport and energy degradation in the ionosphere: Evaluation of the numerical solution, comparison with laboratory experiments and auroral observations, *Ann. Geophys.*, *12*, 1039, 1994.
- Rees, M. H., Excitation of high altitude red auroral arcs, *Planet. Space Sci.*, *8*, 59, 1961.
- Rees, M. H., On the interaction of auroral protons with the Earth's atmosphere, *Planet. Space Sci.*, *30*, 463, 1982.
- Rees, M. H., Physics and Chemistry of the Upper Atmosphere, 289 pp., Cambridge Univ. Press, New York, 1989.
- Rees, M. H., and C. S. Deehr, The aurora of 27 November 1959 at College, Alaska, including observations of a high altitude red arc, *Planet. Space Sci.*, *8*, 49, 1961.
- Rees, M. H., and R. G. Roble, Excitation of O(<sup>1</sup>D) atoms in aurorae and emission of the [OI] 6300-Å line, *Can. J. Phys.*, *64*, 1608, 1986.
- Roble, R. G., The NCAR thermosphere-ionosphere-mesosphere-electrodynamics general circulation model (TIME-GCM), in *STEP Handbook of Ionospheric Models*, edited by R. W. Schunk, p. 281, SCOSTEP Secretariat, Boulder, CO, 1996.
- Rudd, M. E., Energy and angular distribution of secondary electrons from 5 to 100 keV proton with hydrogen and nitrogen molecules, *Phys. Rev. A*, *20*, 787, 1979.
- Semeter, J., and M. Mendillo, Groundbased tomography of atmospheric emissions, *IEEE Trans. Geosci. Remote Sens.*, *35*, 1105, 1997.
- Semeter, J., M. Mendillo, and J. Baumgardner, Multispectral tomographic imaging of midlatitude aurora, *J. Geophys. Res.*, *104*, 24,565, 1999.
- Sigernes, F., Estimation of initial auroral proton energy fluxes from Doppler profiles, *J. Atmos. Terr. Phys.*, *58*, 1871, 1996.
- Sigernes, F., G. Fasel, J. Minow, C. S. Deehr, R. W. Smith, D. A. Lorentzen, L. T. Wetjen, and K. Henriksen, Calculations and ground based observations of pulsed proton events in the dayside aurora, *J. Atmos. Terr. Phys.*, *58*, 1281, 1996.
- Srivastava, V., and V. Singh, Model calculations of O(<sup>1</sup>S) and O(<sup>1</sup>D) emissions under proton bombardment, *J. Geophys. Res.*, *93*, 5855, 1988.
- Strickland, D. J., R. E. Daniell Jr., J. R. Jasperse, and B. Basu, Transport-theoretic model for the electron-proton-hydrogen atom aurora, 2, Model results, *J. Geophys. Res.*, *98*, 21,533, 1993.
- Synnes, S. A., F. Søråas, and J. P. Hansen, Monte-Carlo simulation of proton aurora, *J. Atmos. Sol. Terr. Phys.*, *60*, 1695, 1998.
- Van Zyl, B., M. W. Gealy, and H. Neumann, N<sub>2</sub><sup>+</sup> first negative emission cross sections for low energy H<sup>+</sup> and H impact on N<sub>2</sub>, *Phys. Rev. A*, *28*, 2141, 1983.
- M. Galand and M. J. Mendillo, Center for Space Physics, Boston University, Boston, MA 02215.
- D. Lummerzheim, Geophysical Institute, University of Alaska, Fairbanks, AK 99775-7320.
- M. H. Rees, Physics Department, Southampton University, Southampton, SO17 1BJ, England, UK.
- F. J. Rich, U.S. Air Force Research Lab., Space Vehicle Directorate (RL/VSB), Hanscom AFB, MA 01731-3010.
- J. Semeter, SRI International, Menlo Park, CA 94025.
- February 16, 2000; revised June 9, 2000; accepted June 9, 2000.  
Copyright 2001 by the American Geophysical Union.  
Paper number 2000JA002005.  
10.1029/2000JA002005\$09.00
- 
- This preprint was prepared with AGU's L<sup>A</sup>T<sub>E</sub>X macros v4, with the extension package 'AGU++' by P. W. Daly, version 1.6b from 1999/08/19.